PCCP

Accepted Manuscript

ROYAL SOCIETY OF CHEMISTRY

www.rsc.org/pccp

Spin-Inversion and Spin-Selection in the Reactions

$FeO^+ + H_2$ and $Fe^+ + N_2O$

Shaun G. Ard,[a] Ryan S. Johnson,[b] Joshua J. Melko, [a,c] Oscar Martinez Jr,[a] Nicholas S. Shuman,[a]

Vladimir G. Ushakov,[d,e] Hua Guo,[b] Jürgen Troe,[*,e-g] and Albert A. Viggiano[a]

February 2015

to be published in Phys. Chem. Chem. Phys.

---

[a]Air Force Research Laboratory, Space Vehicle Directorate, Kirtland AFB, New Mexico 87117-5776, USA

[b] Department of Chemistry and Chemical Biology, University of New Mexico, Albuquerque, New Mexico 87131, USA

[c] Department of Chemistry, University of North Florida, Jacksonville, Florida 32224, USA

[d]Institute of Problems of Chemical Physics, Russian Academy of Sciences, 142432 Chernogolovka, Russia

[e] Institut für Physikalische Chemie, Universität Göttingen, Tammannstrasse 6, D-37077 Göttingen, Germany

[f] Max-Planck-Institut für Biophysikalische Chemie, Am Fassberg 11, D-37077 Göttingen, Germany

[g] Laser-Laboratorium Göttingen, Hans-Adolf-Krebs-Weg 1, D-37077 Göttingen, Germany

[*]Email: shoff@gwdg.de

Abstract

The reactions of FeO^+ with H_2 and of Fe^+ with N_2O were studied with respect to the production and reactivity of electronically excited $^4Fe^+$ cations. The reaction of electronic ground state $^6FeO^+$ with H_2 was found to predominantly produce electronically excited $^4Fe^+$ as opposed to electronic ground state $^6Fe^+$ corresponding to a spin-allowed reaction. $^4Fe^+$ was observed to react with N_2O with a rate constant of 2.3 (+0.3/-0.8) x 10^{-11} cm^3 $molecule^{-1}$ s^{-1} , smaller than the ground state $^6Fe^+$ rate constant of 3.2 (±0.5) x 10^{-11} $cm^3molecule^{-1}$ s^{-1} (at room temperature). While the overall reaction of $^6FeO^+$ with H_2 within the Two-State-Reactivity concept is governed by efficient sextet-quartet spin-inversion in the initial reaction complex, the observation of predominant $^4Fe^+$ production in the reaction is attributed to a much less efficient quartet-sextet back-inversion in the final reaction complex. Average spin-inversion probabilities are estimated by statistical modeling of spin-inversion processes and related to the properties of spin-orbit coupling along the reaction coordinate. The reaction of FeO^+ with H_2 served as a source for $^4Fe^+$, subsequently reacting with N_2O. The measured rate constant has allowed for a more detailed understanding of the ground state $^6Fe^+$ reaction with N_2O, leading to a significantly improved statistical modeling of the previously measured temperature dependence of the reaction. In particular, evidence for the participation of electronically excited states of the reaction complex was found. Deexcitation of $^4Fe^+$ by He was found to be slow, with a rate constant < 3 x 10^{-14} cm^3 $molecule^{-1}s^{-1}$.

1. Introduction

Two-State Reactivity (TSR), where excited electronic states of reaction complexes can act to lower intrinsic bottlenecks even in spin-allowed reactions, has proven to be an important concept in understanding numerous organometallic reactions (see, e.g., refs. 1-6). Transition metal ions, due to their abundance of low lying excited states, have figured prominently into both the development and application of this paradigm. The iron cation is perhaps the most studied of the transition metal ions in this context, as it is relatively easy to produce and is of great importance in many biological functions. Likewise, reactions of FeO^+, transferring oxygen atoms to a variety of bonds, have been studied extensively and served as prototype processes in this field.

Fe^+ and FeO^+ both have sextet electronic ground states and low-lying electronically excited quartet states. Colliding sextet Fe^+ and FeO^+ with neutral molecules in singlet electronic ground states, therefore, leads into bound sextet adducts which, however, are separated from reaction products by high energy barriers. These barriers can be circumvented by spin-inversion to quartet adducts which generally have lower barriers towards reaction products. There may be a back-inversion beyond these barriers leading to reaction products in sextet states, which are usually lower in energy. It has been postulated that the second crossing may be significantly less efficient[7,8], yet there are no experiments to determine the product state distribution. The interplay between the initial formation of reaction complexes, spin-inversion and barrier-crossing processes, branching and final dissociation of reaction complexes, leads to a variety of interesting kinetic phenomena which have attracted the attention of many experimentalists and theoreticians.

Among the most studied reactions is the process

$$FeO^+ + H_2 \rightarrow {}^6Fe^+ + H_2O \qquad (1a)$$

$$^4Fe^+ + H_2O \qquad (1b)$$

whose rate has been measured in great detail(see, e.g., refs. 9-14 and earlier work cited therein) and whose molecular properties were studied by high-level quantum-chemical methods (see, e.g., ref. 15 and earlier work cited therein). Statistical rate theory well reproduced absolute values, temperature dependences, and isotope effects of the rate constants when both energy and angular momentum dependences were included. Only single parameters of the potential energy surface to the experiments needed to be fit. The agreement between the statistical analysis of the experiments of ref. 14 and the quantum-chemical results from ref. 15 appears most encouraging such that the present work continues to employ statistical rate modeling. In particular it focuses on an additional aspect of the kinetics, namely on the branching between the channels (1a) and (1b) addressing the question of the second barrier crossing. Thus, it is related to the evolution of the strength of spin-orbit coupling along the reaction coordinate.[7,8]

As explained below, production of $^4Fe^+$ (reaction (1b)) was found to dominate formation of $^6Fe^+$ (reaction (1a)). We, therefore, used the reaction of $^6FeO^+$ with H_2 as a source for electronically excited quartet $^4Fe^+$ cations to measure the rate constant for the reaction of $^4Fe^+$ with N_2O,

$$^4Fe^+ + N_2O \rightarrow FeO^+ + N_2, \qquad (2b)$$

in comparison to that of the well-studied reaction of ground state Fe^+,

$$^6Fe^+ + N_2O \rightarrow FeO^+ + N_2 \qquad (2a)$$

In earlier work[16] we have extended measurements of the temperature dependence of the rate constant of the reaction of Fe^+ with N_2O and analyzed the results by a non-statistical rate model. Given the unique temperature dependence observed, significant effort went into verifying only a ground state contribution to the results. Specifically, the linear decay of the parent ion on a semi-logarithmic plot over several orders of magnitude confirms the absence of any population reacting with a different rate constant. The foregoing article,[17] however, showed that an E- and J-specific statistical rate model with fully or partly efficient spin-inversion could much better reproduce the experimental details. Since the model was not unique, further experimental observations would help to improve the theoretical analysis. Such experiments are described in the present work, measuring the rate of reaction (2b) in comparison to that of reaction (2a). Besides spin-inversion, we find that transitions to electronically excited states of the primary FeN_2O^+ complexes must be involved. In this connection, we mention that the role of excited electronic states of adducts in the capture of open electronic shell species quite generally is underestimated (see, e.g., our recent work on the capture of OH by C in ref. 18).

2. Experimental technique

All experiments were conducted in the variable temperature selected ion flow tube (VT-SIFT) discussed in detail elsewhere (see, e.g., refs. 14 and 16); therefore, only pertinent variations will be discussed here. FeO^+ ions are formed by electron impact ionization upon a gas mixture of $Fe(CO)_5$ and N_2O in He. Ions are then focused before entrance to a quadrupole mass filter where FeO^+ is isolated. Mass selected ions are then further focused by an einzel lens before introduction to the flow tube via a venturi inlet. H_2 is added at a known concentration in one of three inlet ports, located 109, 79, and 69 cm from the end of the flow tube, producing either $^4Fe^+$ or $^6Fe^+$. Ground state FeO^+ was verified by observing linear decay of FeO^+ with respect to H_2 on a semi-logarithmic plot over several orders of magnitude. N_2O is then variably added 59 cm from the end of the flow tube, reacting with Fe^+ to reproduce FeO^+ in a manner similar to our typical kinetic studies.[14, 16] The resulting ions are extracted from the flow tube through a biased graphite nose cone, are mass analyzed by a quadrupole mass spectrometer, and subsequently are detected by a channeltron electron multiplier. The Fe^+ and FeO^+ signals are monitored as a function of N_2O flow, and modeled allowing for a wide array of reactions, see scheme (3).

Scheme (3) is simplified for clarity, with additional chemistry and spin-orbit effects described later in the text. Data were taken under 12 complimentary conditions, varying the amount of H_2 added, which injection port prior to the N_2O injection the H_2 was added, as well as the pressure of the flow tube and, therefore, the total reaction time. Data were then fit using a Monte Carlo optimization procedure described previously.[19] Briefly, product ion concentrations were calculated by iteratively solving the set of differential equations describing reaction scheme (3) for each of the 12 data sets concurrently. The calculated concentrations were compared to the experimental data via a weighted least squares procedure. Rate constants were varied within constraints set either by the literature where available, or limited only by the calculated collisional rate constant otherwise. Additional reactions are considered as discussed below but have a negligible effect on the analysis.

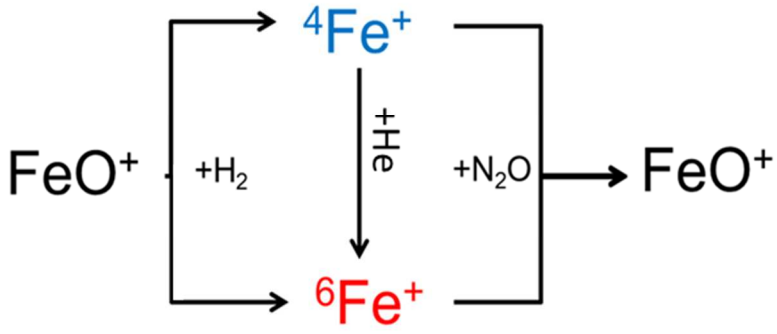

(3)

3. Experimental results

An example set of data at is shown in Fig. 1. The modeling shown as solid curves is the best fit to the data allowing for both reactions (1a) and (1b) while the dashed curves allow for ground state reaction only (reaction 1a). At lower N_2O flows, the Fe^+ decay is equally reproduced by either fit but at high N_2O modeling with only one state of Fe^+ underestimates the data. The effect is subtle but is consistently reproduced in data sets of varied H_2 concentration and inlet port, collision frequency, and total reaction time. The conclusions presented herein are based on simultaneous fitting of 12 representative sets of data at varied conditions, lending statistical weight to this seemingly minor effect as explained below.

In order to determine rate constants for the two states, the least squares parameter determined in the Monte Carlo fitting is plotted in Fig. 2 as a function of the rate constant for both $^4Fe^+$ and

$^6Fe^+$; the former shown in red and the latter in blue. The minima of the "dot" plots correspond to the best values for the rate constants. The plot shows that the rate constants are well defined and separate, with the quartet rate constant smaller than that for the sextet. The most probable rate constant, k_{2b} = 2.3 (+0.3/-0.8) x 10^{-11} cm^3 $molecule^{-1}$ s^{-1}, is surprisingly smaller than that for the reaction of $^6Fe^+$, being[16] k_{2a} = 3.2 (±0.5) x 10^{-11} cm^3 $molecule^{-1}$ s^{-1}. That is why the data curve upwards more than the single state model. While the absolute rate constants have enough uncertainty to think of these as overlapping, the results shown in Fig. 2 indicates that they do not. Armentrout et al[20,21] and Weisshaar et al[22,23] have studied the reactivity of $^4Fe^+$ and $^6Fe^+$ for numerous systems, finding the quartet state to typically react more efficiently. In the reaction of Fe^+ with propane,[21] however, Armentrout found that at low energies the ground sextet state did indeed react faster, just as in the present case, while at higher energies the excited quartet state reverted to the more efficient reactant, highlighting the complex nature of the problem. In fact, individual spin orbit states have often been observed to react differently,[20-25] a point which will be discussed later in the text. The measured value of k_{2b} in addition to our earlier value of k_{2a} has shed insight into our understanding of the ground state $^6Fe^+$ reactivity for this system, see our previous article[17] and the discussion given below.

In order for the experiment to distinguish the reactivity of the two states, the quenching rate for $^4Fe^+$ to $^6Fe^+$ by He must be comparable or slower than the reaction time. Oriedo et al[26] have studied collisional relaxation of exited states of Fe^+ with numerous collision partners. They found $^4Fe^+$ to be poorly quenched relative to other excited states, especially by He. In the present experiments, we varied reaction time and collision frequency to determine this quenching rate. A subset of the Monte Carlo runs showing the best fits for this quenching rate constant is shown in Fig. 3. The previously value reported by Oriedo is shown by the red dotted line near to 3 x 10^{-12} $cm^3molecule^{-1}$ s^{-1}. Clearly the present data is best modeled by a significantly lower value. Employing a least squares cutoff of 10^{-5}, for reasons to be discussed further on, we cautiously set a limit of < 3 x 10^{-14} cm^3 $molecule^{-1}s^{-1}$ for the quenching rate, i.e. too slow to have a large effect on the data and in reasonable agreement with Bowers et al's determination of 4 (±2) x 10^{-14} cm^3 $molecule^{-1}s^{-1}$.[27]

In addition to the reactions shown in scheme (3), other reactions were included to test the sensitivity of the present conclusions. FeO^+ is known[16] to cluster with N_2O up to a coordination

number of 3. The wide variety of reaction times and He densities employed allowed for the determination of a third order rate constant of 1.8 (±0.3) x 10^{-27} cm^6 $molecule^{-2}s^{-1}$ for the initial N_2O association, in reasonable agreement with our previous measurements.[16] Additionally, reaction of these clusters with H_2 to directly reproduce Fe^+ was allowed and found to have no bearing on the present results, with an effective rate constant ≤ 10^{-13} cm^3 $molecule^{-1}s^{-1}$ The Monte Carlo plots shown in this work include the contributions of this chemistry. No other ions were observed, and thus no unaccounted for chemistry is likely to explain the observed effects. Furthermore, the possibility of $^4FeO^+$ influencing the present results was considered. The rate constant of reaction (1) was tightly optimized to 1.05 x 10^{-11} cm^3 $molecule^{-1}s^{-1}$, in excellent agreement with our previously measured value of 1.0 (±0.25) x 10^{-11}.[14] This implies that either no $^4FeO^+$ was formed, or that quenching of this state was too fast for it to affect the present results.

The least squares plot for the branching of $^6FeO^+ + H_2$ towards $^4Fe^+$ in reaction (1b) is shown in Fig. 4. The best fits to the data are with mainly formation of $^4Fe^+$ and little formation of ground state $^6Fe^+$ from reaction (1a). This value of the quartet yield is somewhat broadly determined, as the branching determination is intimately tied to the value of the excited state rate constant k_{2b}. It is clear, however, that a branching of zero, i.e. sole production of ground state $^6Fe^+$, would result in a much poorer fit to the data, as also evidenced in Fig 1. This is perhaps not surprising. Quantum-chemical calculations of the strength of spin-orbit coupling along the reaction coordinate[7,8] showed that the coupling greatly weakens as one proceeds from reactants to products. This result will be further discussed below.

The error limits for the values determined by the present experiments merit discussion. The general manner in which error limits are determined from the Monte Carlo optimization procedure involve an "eye test" to determine the weighted least squares parameter, or "goodness", at which the model no longer adequately represent the data. Values producing a "goodness" value less than this determined number are then within the uncertainty limits of the optimization. This works well when individual data sets are analyzed independently but is quite difficult in the present case as up to 9 data sets were run cumulatively making determination by eye quite daunting. The determined rate constant for $^4Fe^+$ with N_2O, however, allows us to set

error limits due to the limited values for this parameter providing the best fits. While this value was varied from 10^{-13} to 10^{-9} cm^3 $molecule^{-1}$ s^{-1}, the range from $1.5 \times 10^{-11} \leq k_{4Fe+} \leq 2.6 \times 10^{-11}$ cm^3 $molecule^{-1}$ s^{-1} resulted in the best fits to the data, and therefore a least squares parameter of 10^{-5} was chosen as the value where other error limits were determined. The best fits are with a branching in reaction 1 from 0.75 to 1, however, this branching and the rate constant for reaction 2b cannot completely be decoupled. This is shown clearly in Fig. 5 where a contour plot of the least squares parameter is shown with branching on the y-axis and k_{2b} on the x-axis. The best least squares parameter is shown in red and occurs along a diagonal ranging from a branching of 0.75 to 1. Higher branching is associated with faster rates for the quartet state. The dark blue contour is our error limit, leading to a somewhat overly cautious limit of ≥ 0.4 for the branching of reaction (1) to $^4Fe^+$.

4. Statistical modeling of rate constants for the reactions $^4Fe^+ + N_2O$ and $^6Fe^+ + N_2O$

The lowest fine-structure levels of $Fe^+(^4F)$ and $Fe^+(^6D)$ are 1872.6 cm^{-1} apart.[28]. At first sight, therefore, it appears surprising that the energetically higher species $^4Fe^+$ should react slower with N_2O than $^6Fe^+$. In the preceding article,[17] the experimental values for the sextet rate constants k_{2a} from ref. 16 were fitted by simple statistical modeling., Values of the quartet rate constant were found to be larger than those for the sextet, $k_{2b} > k_{2a,}$ independent of the choice of the model. A way out of this dilemma was the suggestion that electronically excited adduct potentials contribute to the overall reaction to a larger extent for the $^6Fe^+$ reactant than for $^4Fe^+$. Fig. 6 schematically illustrates this hypothesis for one potential possibility. In the shown example, all of the 5 sextet potentials originating from $^6Fe^+$ are assumed to cross the bonding quartet potential at energies accessible in the thermal experiments and, after spin-inversion, continue to proceed over the quartet transition state with each state having essentially the same crossing probability. In contrast, only one of the 7 quartet adduct potential energy surfaces originating from the fine-structure levels of $^4Fe^+$ are assumed to lead into a sufficiently bound quartet adduct INT1, and then proceed over the quartet transition state ^4TS to products. As the fitting of the experimental data is not unique, it is by no means certain that only a single quartet and all sextet

surfaces contribute to the reaction. The experimental data, nevertheless, strongly suggest that only a minor fraction of the quartet and a major part of the sextet states are of major significance. In detail, the diagram of Fig. 6 should be understood in the following way. At large ion-neutral distances, all potentials originating from the Fe^+ fine-structure levels are more or less parallel to each other and are attractive. At shorter distance, i.e. in the valence region of the interaction between the reactants, 5 sextet and 7 quartet adduct potentials are formed which may be either attractive or repulsive. To get to products the sextet states usually (sextet barrier is near zero) cross to the quartet surface and then pass through the lower energy quartet barrier to products. The quartet state has sufficient energy to easily cross either barrier, yet the data show that the quartet states react slower. Our analysis cannot distinguish the exact shape of the potentials. The true description depends heavily on details of each individual crossing seam; how efficient the crossing, as well as where the seam is energetically relative to the transitions state. Computational treatment of this multitude of crossing seams is daunting, but would allow for significant enhancement of the simplified model presented here, and therefore would be highly desirable.

Following the statistical method outlined in the foregoing article,[17] here we further elaborate the statistical modeling of the rate constants k_{2a} and k_{2b}. In particular, instead of working with fine-structure averaged levels, we have distinguished all fine-structure levels[28] and repeated the parameter optimization, comparing the results either with a contribution from single sextet and quartet potentials (case 1) or with 5 sextet plus a single quartet potential (case 2). In both examples optimum fits to the experimental sextet rate constants k_{2a} could be derived although with different fitting parameters. However, the two models differ in the corresponding value for k_{2b}. Fig. 7 shows the quality of the data representation. Fits to the sextet reactant are shown as solid red and green and essentially overlap for case 1 and 2, respectively. As indicated previously,[17] the choice of parameters obtained from fitting the data for k_{2a} is not unique. However, including fits to the experimental k_{2b} does make the choice of parameters clear. The dashed red and green curves are fits to k_{2b} for case 1 and 2, respectively. Case 2 fits the data well and case 1 does not come close. Like in ref. 17, finite spin-inversion rates in the adduct INT1 are assumed with effective numbers of states W_{SQ} at the quartet-sextet crossing seams. The black

curve is case 2 with averaged fine-structure states corresponding to fast spin inversion (for further details, see Section 5 of this article). The following optimum parameter sets were obtained: [E(^{4}TS), E(^{6}TS), J_{max}, W_{SQ}] = [-1577 cm^{-1}, +44 cm^{-1}, 98, 299], [-2214 cm^{-1}, +218 cm^{-1}, 59, 3059], [-2861 cm^{-1}, +352 cm^{-1}, 53, 1481] for the red, black, and green lines, respectively. These parameter sets in turn lead to k_{2b} = 7.0 x 10^{-11}, 2.6 x 10^{-11}, and 2.0 x 10^{-11} cm^3 molecule^{-1} s^{-1}, respectively. As emphasized before, the parameter fits are not unique; the variation of the derived parameters reflects the uncertainty. Without assuming only partial contributions of the quartet potentials, $k_{2b} < k_{2a}$ could not be obtained. The measured value of k_{2b} (in addition to k_{2a}), on the other hand can well be reproduced within experimental accuracy with the latter two parameter sets. These both led to a markedly negative quartet ^{4}TS energy and in a small positive ^{6}TS energy. The quantum-chemical energy values from the DFT calculations of ref. 17, such as given in Fig.6, within the uncertainties of both approaches appear consistent with the fitting results.

The fitted values of W_{SQ} are large, but probably not large enough to correspond to complete equilibration of sextet and quartet INT1 (see the discussion in ref. 17 and in Section 5 below). At this stage we have no experimental access to W_{SQ} beyond the fact that the experimental temperature dependence and absolute values of k_{2a} are well reproduced by the modeling with fitted parameters for E(^{4}TS) and E(^{6}TS) consistent with the DFT calculations. If one had measurements of sextet vs quartet FeO^+ production in reaction (2), W_{SQ} could be more directly deduced. Contrary to reaction (1), the branching between reactions (2a) and (2b) most probably occurs in the primary adduct INT1(reactant complex) while additional branching in the product complex, INT2, should be less important, analogously to reaction (1). Because of the much higher energy of the sextet transition state ^{6}TS, sextet product formation in reaction (1) almost exclusively arises from spin-inversion in INT3 (product complex). In contrast, the much lower ^{6}TS energy points to sextet production in reaction (2) being governed by spin-inversion in INT1 (reactant complex) as characterized by the value of W_{SQ}. Fig. 8 illustrates this behavior by showing the calculated contributions to k_{2a} from passage over ^{6}TS and ^{4}TS (leading to sextet and quartet FeO^+ formation). The corresponding red and black lines were calculated using the third

parameter set given above (i.e. [-2861 cm^{-1} , + 352 cm^{-1} , 53, 1481]) which well reproduced the experimental $k_{2a}$and k_{2b}.

5. Simplified statistical model of spin-inversion rates

The present experiments are in several ways connected to the rates of spin-inversion. First, it governs the branching between $^4Fe^+$ and $^6Fe^+$ products of reaction (1) in the late intermediate INT3 of the reaction, see Fig.1 of ref. 14, and it is related to the change of the spin-orbit coupling strength along the reaction coordinate as elaborated in refs. 7 and 8. On the other hand, it is related to the lifetime of INT3. We discuss below the relation of these previous results with the present fitted spin-inversion parameters. Secondly, there is the question of the extent of equilibration between ^{6}INT1 and ^{4}INT1 in the primary adduct of reaction (2). This again is connected to the efficiency of spin-inversion in relation to the lifetime of INT1 for reaction (2) as calculated with the fitted parameters from the experimental results of ref. 17.

As the lifetimes τ of INT1 and INT3 for reaction (1) and of INT1 for reaction (2) are of relevance, we first calculate these quantities. We express them through the average rate constants $<k> = 1/\tau$ for disappearance of the INT as modeled by statistical rate theory employing quantum-chemically calculated and experimentally fitted molecular parameters from refs. 14 and 17. Fig. 9 shows the results for INT1 and INT3 of reaction (1), while Fig.5 of ref. 17 gave the results for INT1 of reaction (2). Fig.9 illustrates the two extremes of fully efficient and fully inefficient equilibration of sextet and quartet adducts INT1 in reaction (1) (one notes a small difference between ortho and para hydrogen due to different populations of entrance states of the reaction). In any case, the <k> are smaller than the smallest vibrational frequencies of INT1 (as derived from DFT calculations, see Appendix), such that spin-inversion probabilities smaller than unity still may allow for a full equilibration of sextet and quartet adducts. Similar calculations for INT3 are included in Fig. 9 (under the assumption of full equilibration of sextets and quartets in INT1; the small difference between ortho and para hydrogen here has almost disappeared.

Because of the larger vibrational energy, <k> is larger for INT3 than for INT1, but still is smaller than the smallest vibrational frequency).

Whether the results for <k>, such as modeled with statistical theory with experimentally fitted parameters, correspond to full or only partial equilibration, depends on the rates of spin-inversion. In statistical modeling we represent these in a simplified manner in the form

(4a) $k_6 = W_{SQ}/h\rho_6$

and

(4b) $k_4 = W_{SQ}/h\rho_4$

for transitions from sextet to quartet and from quartet to sextet states with the vibrational densities of states ρ_6 and ρ_4 .W_{SQ} denotes effective numbers of activated complex states for spin-inversion and in ref. 17 it was taken as an E- and J- independent fitting parameter. In the following we further discuss the meaning of W_{SQ}.

Spin-inversion takes place when the sextet and quartet potentials cross along some crossing seam. Considering non-degenerate potentials, the number of states in contact with this crossing is denoted by $W_x(E,J)$. If there are s contributing sextet and q contributing quartet potentials, the rate constants k_6 and k_4 are written in the form

(5a) $k_6 = s\, W_x\, P(s\rightarrow q)/h\rho_6$

and

(5b) $k_4 = q\, W_x\, P(q\rightarrow s)/h\rho_4$

Obviously, eqs. (5a) and (5b) represent a considerable simplification by treating all crossings in the same way. However, as long as more details are not known, this may appear acceptable. P(s→ q) and P(q→ s) are the average transition probabilities for sextet-quartet and quartet-sextet transitions, obeying microscopic reversibility in the form

(6a) $P(s \rightarrow q) = q\ p$

and

(6b) $P(q \rightarrow s) = s\ p$

The parameter p (assumed to be small) may be understood as the transition probability between non-degenerate states and can be modeled as an average Landau-Zener probability. With these conventions, eq. (4) is obtained with the parameter W_{SQ} given by

(7) $W_{SQ} = s\ p\ q\ W_x$

At this stage, the two problems of estimating p and W_x in eq. (7) can only be approached qualitatively. Based on the calculation of spin-orbit-coupling matrix elements, <SOC>, along the reaction coordinate of reaction (1) by Danovich and Shaik[7], Harvey and Tew[8] have estimated the product s q p, for INT1 in reaction (1), to be about 0.1 for small (as relevant here) and 0.05 for large energies. With s q = 24, the Landau-Zener probability p thus should be of the order of $p \approx 0.005$. In the perturbation limit of Landau-Zener theory, p is proportional to $\langle SOC \rangle^2 / v\ f$ where v is the velocity of crossing the seam and f is the difference of slopes of the two potentials.

Moving from INT1 to INT3 in reaction (1), $\langle SOC \rangle^2$ in INT3 was estimated to drop by about a factor of 16 from the value of INT1, while the velocity at the crossing in INT3 is about 4 times larger than in INT1. As the crossing of the potentials should be located close to the minimum in INT3, the difference in the slopes should be smaller than in INT1. This suggests that p in INT3 should be roughly 50 times smaller than in INT1 and be of the order of 0.0001. An estimation of W_x at this stage is similarly crude. Quantum-chemical calculations[8] showed that sextet and quartet potentials in INT3 cross almost at the bottom of the wells at $E \approx -24000\ cm^{-1}$ (neglecting the entrance thermal energy). If one assumes that the two potentials have similar properties near to the bottoms and that the smallest frequency corresponds to the motion across the crossing seam, then W_x is roughly estimated by the number of states of the remaining five oscillators of INT3 which is given by $W_x \approx (2J + 1)\, E^5 /5!\, \Pi^*(\omega_i)$ where the product $\Pi^*(\omega_i)$ includes the frequencies of the five remaining oscillators. W_x then is about $(2J + 1)10000$ and $W_{SQ} \approx p\,(2J + 1)\, 240000 \approx (2J + 1)\, 24$.A rough estimate of the relevant J is obtained from the thermally averaged value $0.6\{(T/K)/(B/cm^{-1})\}^{1/2} \approx 40$ (with $B/cm^{-1} \approx 0.06$, see ref. 17, and T/K=300). This leads to the crude estimate of $W_{SQ} \approx 2000$, which appears compatible with the fitted values given above, see section 4. Unfortunately analogous estimates for INT1 in reactions (1) and (2) are even less meaningful. Nevertheless, crude estimates of W_{SQ} such as demonstrated here appear compatible with values for reaction (2) as fitted experimentally.

6. $^4Fe^+$ / $^6Fe^+$ branching ratios in reaction (1)

The transition state for direct formation of $^6Fe^+$ from INT1 in reaction (1) has such a high energy that $^6Fe^+$ formation only from ^{6}INT3 after spin-inversion from ^{4}INT3 has to be considered. One may also assume that steady state between ^{4}INT3 and ^{6}INT3 will be established. Denoting the population of ^{6}INT3 at a given J and in an energy interval (E, E + dE) by c_6 and the corresponding population of ^{4}INT3 by c_4, steady state between ^{6}INT3 and ^{4}INT3 for the population of ^{6}INT3 leads to the relation

(8) $c_4 k_4 = c_6 k_6 + c_6 W_6 / h \rho_6$

where the terms with k_4 and k_6 correspond to spin-inversion steps and the last term at the rhs corresponds to dissociation of ^{6}INT3 towards products. On the other hand the branching ratio ^{6}BR for formation of $^6Fe^+$ from INT3 is given by the ratio of dissociation fluxes from INT3,

(9) $^6BR = c_6 W_6 / h \rho_6 \; / (c_6 W_6 / h \rho_6 + c_4 W_4 / h \rho_4)$

Combining eqs. (4), (8) and (9), gives

(10) $^6BR = W_6 W_{SQ} / [W_6 W_{SQ} + W_4 (W_6 + W_{SQ})]$

At the energies of relevance and for a lower energy threshold for formation of $^6Fe^+$ than for $^4Fe^+$, one can easily estimate the ratio W_6/W_4, being about 2.5. Representing W_{SQ} as described in Section 5, leads to a qualitative estimate between experimental branching ratio ^{6}BR and the average spin-inversion probability p. For example, a branching ratio of ^{6}BR = 0.1 corresponds to p = 0.01. According to eq. (10), smaller values of ^{6}BR correspond to even smaller values of p. The qualitative estimate of $p \approx 0.0001$ from Section 5, with $W_6/W_4 \approx 2.5$, $W_6 \approx 40000$, and $W_{SQ} \approx 20$, according to eq.(10) leads to $^6BR \approx 0.001$, consistent with the experimental results. .

6. Conclusions

The present work has employed sequential reactivity to study the production of excited Fe^+ from H_2 reacting with FeO^+, reaction (1), and the subsequent reactivity of $^4Fe^+$ with N_2O, reaction (2b). Reaction (1) was found to produce primarily $^4Fe^+$, though the intimate coupling of this branching to both the quenching rate and reactivity of this ion leads to a cautiously set a limit of

> 0.40 for ^{4}BR in reaction (1). The rate constant for reaction (2b), however, was well determined by the present experiments, finding a value of 2.3(+0.3/-0.8) x 10^{-11} cm^3 $molecule^{-1}$ s^{-1}.

We have rationalized the experimental observation of predominant formation of $^4Fe^+$ in reaction (1) in terms of spin-orbit coupling matrix elements and Landau-Zener spin-inversion probabilities from refs. 7 and 8. The relation could be established by statistical modeling of spin-inversion rate constants, although the absence of more information on quartet-sextet crossing seams only allowed for qualitative estimates.

Finally, statistical rate modeling was also successfully applied to reaction (2). The smaller reactivity of $^4Fe^+$ in comparison to that of $^6Fe^+$, however, could not be explained without the additional assumption that only a minority of the manifold of electronic states originating from the interaction between $^4Fe^+$ and N_2O contributes to the reaction whereas at least the major part of the manifold originating from $^6Fe^+$ after spin-inversion can react. Evaluating the experimental results by the statistical modeling leads to fitted energy parameters which appear consistent with quantum-chemical calculations when the remaining uncertainties of the latter and the simplicity of the approach are taken into consideration.

While branching between sextet and quartet products in reaction (1) is governed by spin-inversion in the late complex INT3 of the reaction, the branching between sextet and quartet products in reaction (2) arises from spin-inversion in the early adduct INT1. This difference in behavior can be attributed to the large difference between the heights of the sextet transition states along the reaction path.

7. Acknowledgments

The authors would like to thank Peter Armentrout, Helmut Schwarz, Sason Shaik, and Jeremy Harvey for insightful conversations. This work is supported by the Department of Energy Office

of Science, Office of Basic Energy Research (DE-FG02-05ER15694 to H.G.) and by the Air Force Office of Scientific Research (AFOSR-2303EP to A.A.V.). S.G.A. acknowledges the support of Boston College Institute of Scientific Research. J.T. acknowledges support from the EOARD Grant-Award FA8655-11-13077.

References

1 S. Shaik, D. Danovich, A. Fiedler, D. Schröder and H. Schwarz, Helv. Chim. Acta, 1995, **78**, 1393 – 1407.

2 D. Schröder, S. Shaik and H. Schwarz, Acc. Chem. Res., 2000, **33**, 139 – 145.

3 S. Shaik, Int. J. Mass Spectrom., 2013, **354**, 5 – 14.

4 D. K. Böhme and H. Schwarz, Angew. Chem. Int. Ed., 2005, **44**, 2336 – 2354.

5 P. B. Armentrout, Annu. Rev. Phys. Chem., 2001, **52**, 423 – 461.

6 D. Schröder and H. Schwarz, Angew. Chem. Int. Ed., 1995, **34**, 1973 – 1975.

7 D. Danovich and S. Shaik, J. Am. Chem. Soc., 1997, **119**, 1773 – 1786.

8 J. N. Harvey and D. P. Tew, Int. J. Mass Spectrom., 2013, **354 -355**, 263 – 270.

9 D. Schröder, A. Fiedler, M. F. Ryan and H. Schwarz, J. Chem. Phys., 1994, **98**, 68 – 70.

10 D. E. Klemmer, Y. M. Chen, F. A. Khan and P. B. Armentrout, J. Phys. Chem., 1994, **98**, 6522 – 6529.

11 D. Schröder, H. Schwarz, D. E. Clemmer, Y. M. Chen, P. B. Armentrout, V. I. Baranov and D. K. Bohme, Int. J. Mass Spectrom. Ion Process., 1997, **161**, 175 – 191.

12 M. Filatov and S. Shaik, J. Phys. Chem. A, 1998, **102**, 3835 – 3846.

13 J. M. Matxain, J. M. Mercero, A. Irigoras and J. M. Ugalde, 2004, **102**, 2635 – 2637.

14 S. G. Ard, J. J. Melko, O. Martinez Jr., V. G. Ushakov, A. Li, R. S. Johnson, N. S. Shuman, H. Guo, J. Troe and A. A. Viggiano, J. Phys. Chem. A, 2014, **118**, 6789 – 6797.

15 A. Altun, J. Breidung, F. Neese and W. Thiel, J. Chem. Theory Comput. 2014, **10**, 3807 – 3820.

16 J. J. Melko, S. G. Ard, J. A. Fournier, J. Li, N. S. Shuman, H. Guo, J. Troe and A. A. Viggiano, Phys. Chem. Chem. Phys. 2013, **15**, 11257 – 11267.

17 S. G. Ard, H. Guo, R. S. Johnson,N. S. Shuman, J. Troe, V. G. Ushakov and A. A. Viggiano, Phys. Chem. Chem. Phys., preceeding article.

18 A. I. Maergoiz, E. E. Nikitin and J. Troe, J. Chem. Phys., 2014, **141**, 044302.

19 N. S. Shuman, T. M. Miller, A. A.Viggiano and J. Troe, Adv. At. Mol. Opt. Phys, 2012, **61**, 209 – 294.

20 J. L. Elkind and P. B. Armentrout, J. Phys. Chem., 1986, **90,** 5736 – 5745.

21 R. H. Schultz and P. B. Armentrout, J. Phys. Chem., 1987, **91**, 4433 – 4435.

22 S. D. Hanton, R. J. Noll and J. C. Weisshaar, J. Phys. Chem., 1990, **94**, 5655 – 5658.

23 S. D. Hanton, R. J. Noll and J. C. Weisshaar, J. Chem. Phys., 1992, **96**, 5176 – 5190.

24 K. Tanaka, J. Durup, T. Kato and I. Koyano, J. Chem. Phys., 1980, **73**, 586 – 588.

25 F. Dong, S.-H. Lee and K. Liu, J. Chem. Phys., 2001, **115**, 1197 – 1204.

26 D. H. Russell, T. Solouki and J. V. B. Oriedo, J. Am. Soc. Mass Spectrom., 1995, **6**, 543 – 553.

27 P. A. M. Van Koppen, P. R. Kemper, and **M.T.** Bowers, J. Am. Chem. Soc., 1992, **114**, 10941-10950

28 C. E. Moore, Atomic Energy Levels Vol II (NSRDS-NBS 35, Washington,**1971**).

Appendix Molecular parameters for reaction (1)

Part of the molecular parameters for reaction (1) required in the present statistical modeling, together with a description of the methods of calculation, have been given in ref. 17 and need not to be repeated here. The present calculations of lifetimes of INT1 and INT3 of reaction (1), in addition, need the vibrational frequencies (in cm^{-1}) given in the following.

Vibrational frequencies

INT1(6): 218.1, 234.9, 716.7, 826.0, 976.0, 4080.3; INT1(4): 403.7, 631.6, 984.1, 1039.9, 1482.7, 3495.6; INT3(6): 342.6, 428.6, 559.4, 1680.3, 3749.9, 3833.1; INT3(4): 410.6, 430.7, 673.9, 1694.8, 3774.9, 3849.7.

Figure Captions

Fig.1 FeO^+ (red dots) and Fe^+ (blue squares) signals in the reaction $Fe^+ + N_2O \rightarrow FeO^+ + N_2$ (dashed curves: modeling allowing only for reaction (1a), solid curves: modeling allowing for reactions (1a) and (1b), see the text).

Fig.2 Monte Carlo optimization of the reaction mechanism with respect to the reactions (2a) and (2b) (see the text).

Fig. 3 Monte Carlo optimization of the reaction mechanism with respect to the rate constant of electronic quenching of $^4Fe^+$ by He (see the text).

Fig. 4 Monte Carlo optimization of the reaction mechanism with respect to the branching ratio $^4Fe^+/(^4Fe^+ + {}^6Fe^+) = k_{1b}/(k_{1a} + k_{1b})$ in the reaction $FeO^+ + H_2 \rightarrow Fe^+ + H_2O$ (see the text).

Fig. 5 Cumulative Monte Carlo optimization of the reaction mechanism with respect to the branching ratio $^4Fe^+/(^4Fe^+ + {}^6Fe^+) = k_{1b}/(k_{1a} + k_{1b})$ in reaction (1) and the rate constant k_{2b} of reaction (2b) (see the text).

Fig. 6 Potential energy diagram for reactions (2a) and (2b) , see ref. 7 (schematic representation of the 7 quartet and 5 sextet potentials originating from $^4Fe^+$ and $^6Fe^+$, respectively; see the text).

Fig.7 Rate constants for the reaction $Fe^+ + N_2O$ (● : experimental points for k_{2a} from ref. 11,O : experimental point for k_{2b}, solid curves: modeling of k_{2a} , dashed curves: modeling of k_{2b} , red curves: modeling with 1 sextet and 1 quartet potential , the parameters $[E(^4TS), E(^6TS), J_{max}, W_{SQ}] = [-1577\ cm^{-1}, 44\ cm^{-1}, 98, 299]$ and detailed fine-structure electronic partition functions , black curves: modeling with 5 sextet and 1

quartet potentials, [- 2214 cm^{-1}, + 218 cm^{-1}, 59, 3059] and averaged fine-structure partition functions, green curves: modeling with 5 sextet and 1 quartet potentials, [- 2861 cm^{-1}, + 352 cm^{-1}, 53, 1481] and detailed fine-structure partition functions; see the text).

Fig.8 As Fig. 7 and for the parameter set of the green curves of that figure (green solid curve: sextet rate constant k_{2a} , green dashed curve: quartet rate constant k_{2b}) ; contributions to k_{2a} from reaction over ^{4}TS (black solid curve) and over ^{6}TS (red solid curve).

Fig. 9 Average decay rate constants of INT1 in the reaction $FeO^+ + H_2$ (black curves: ortho-H_2 , red curves para-H_2 , solid curves: full equilibration of sextet and quartet INT1, dashed curves: no equilibration, i.e. only reaction of ^{6}INT1); the same for INT3 (results for full equilibration, the blue curve for para-H_2 and the green curve for ortho-H_2 are nearly indistinguishable).

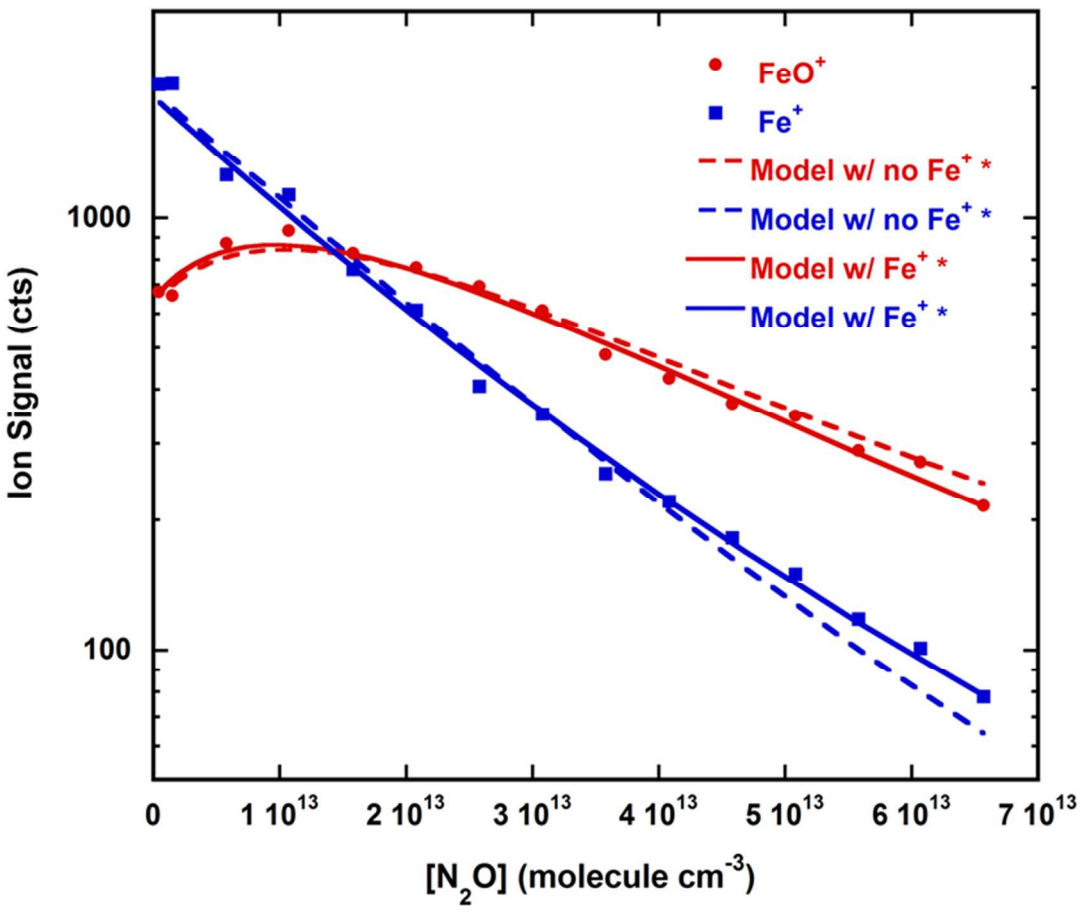

Fig.1

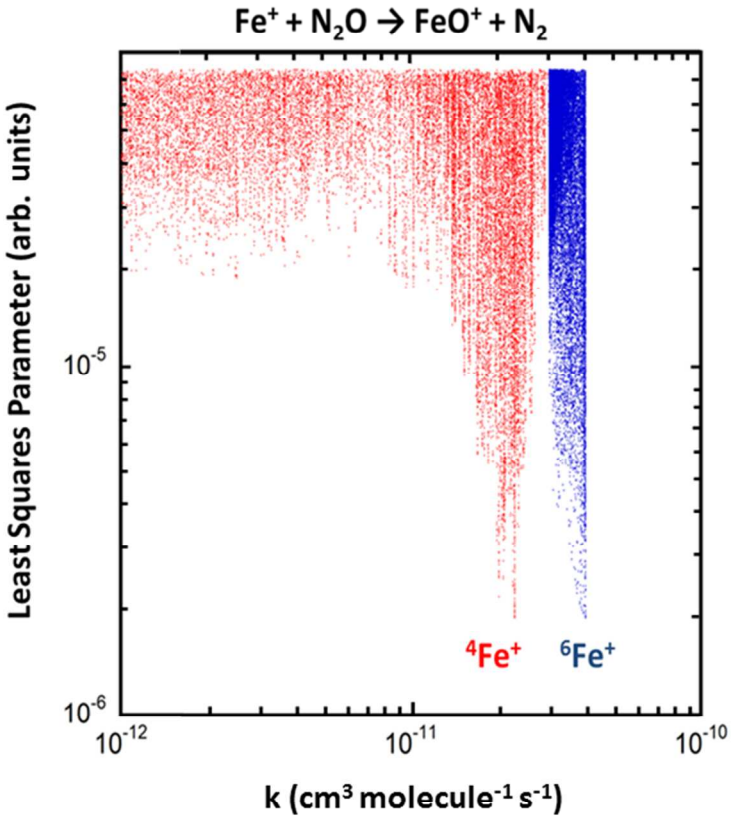

Fig. 2

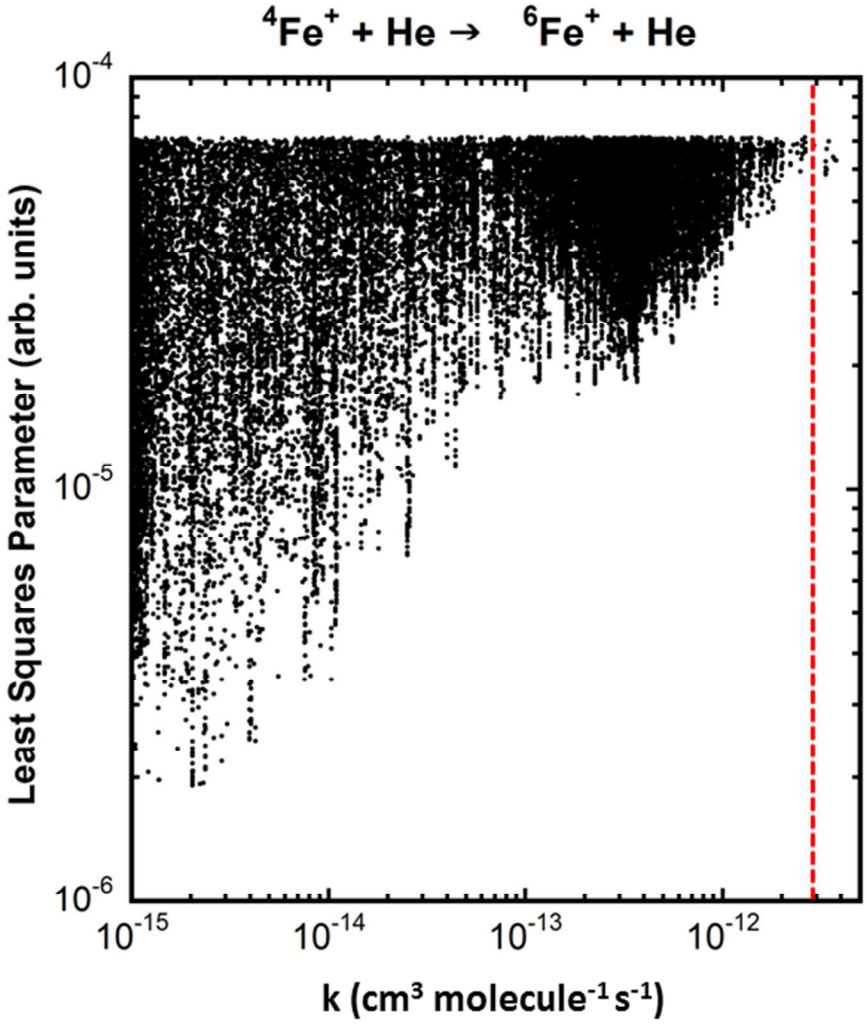

Fig. 3

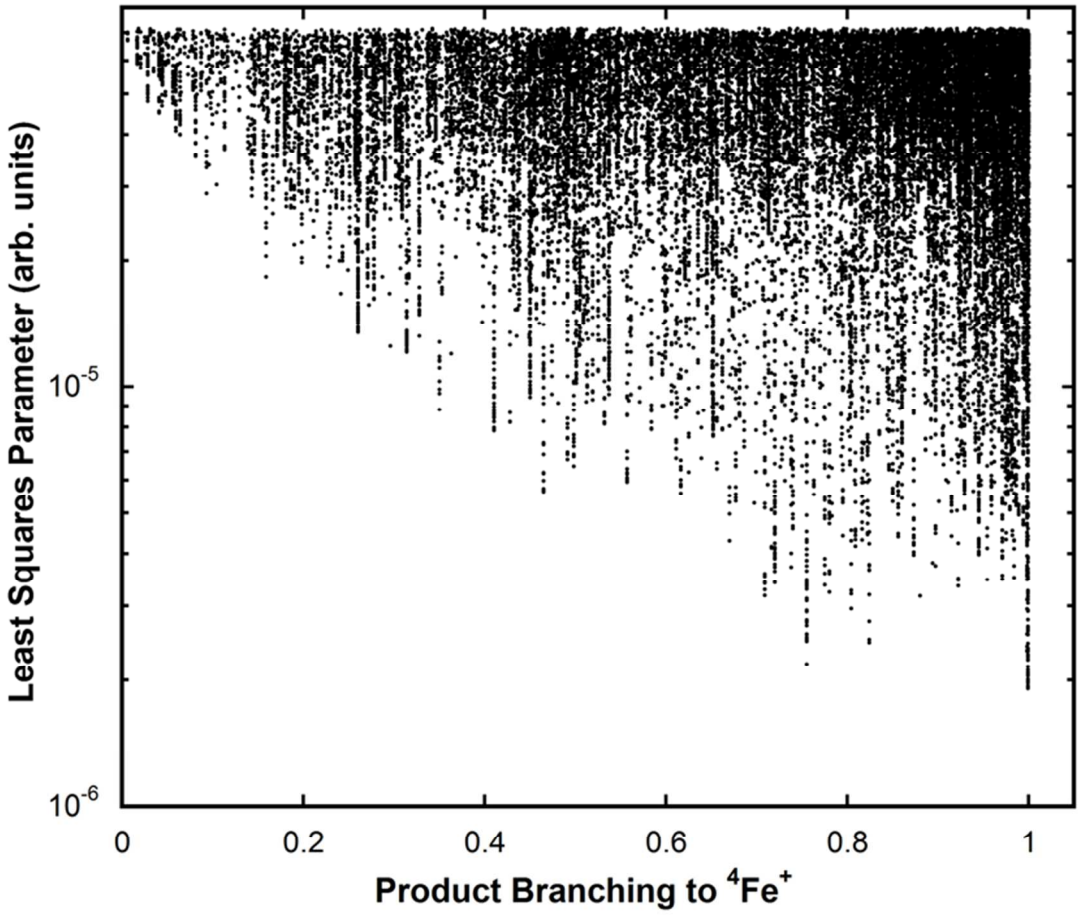

Fig. 4

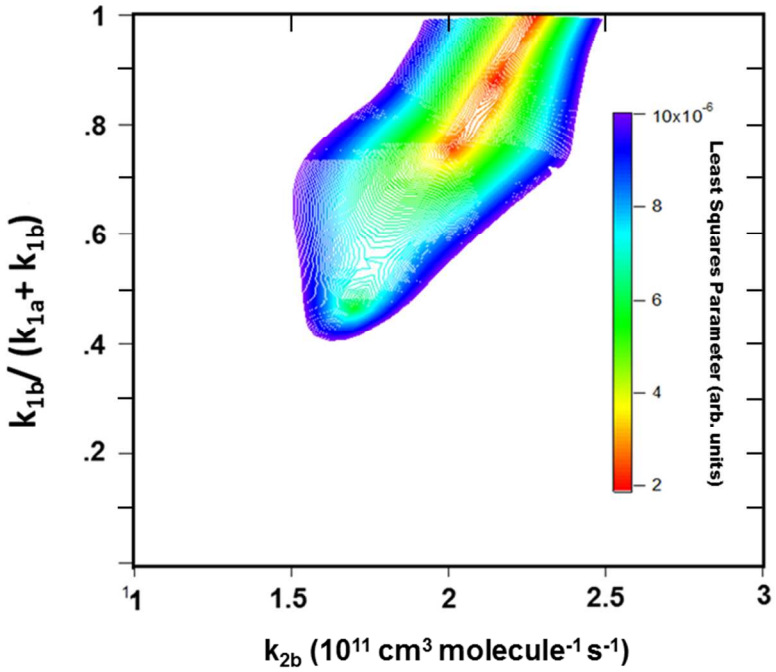

Fig.5

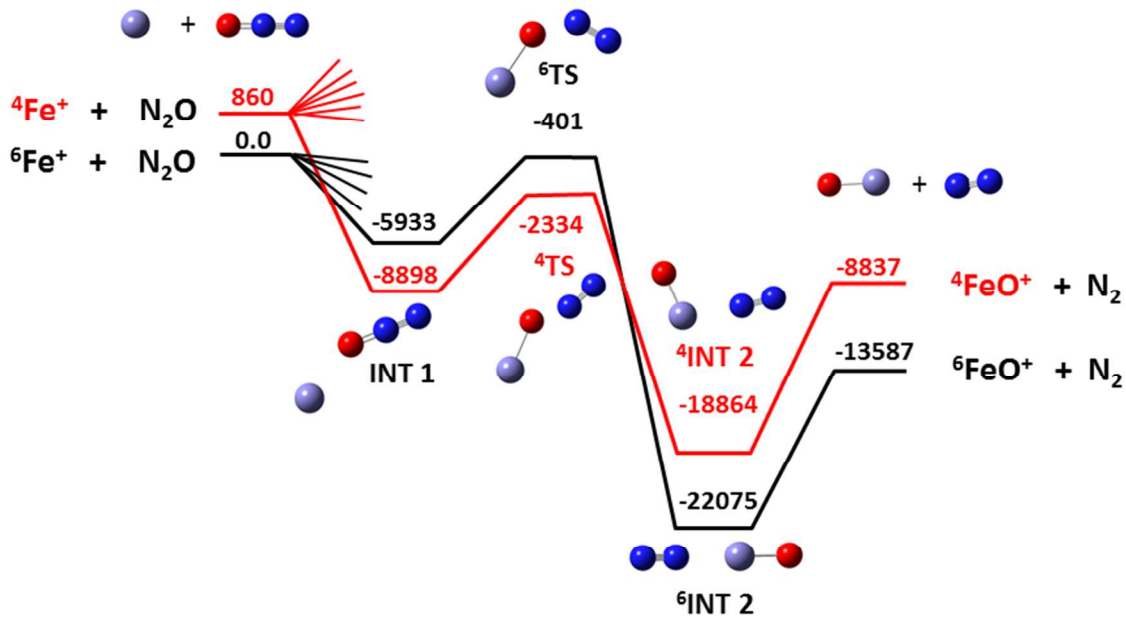

Fig.6

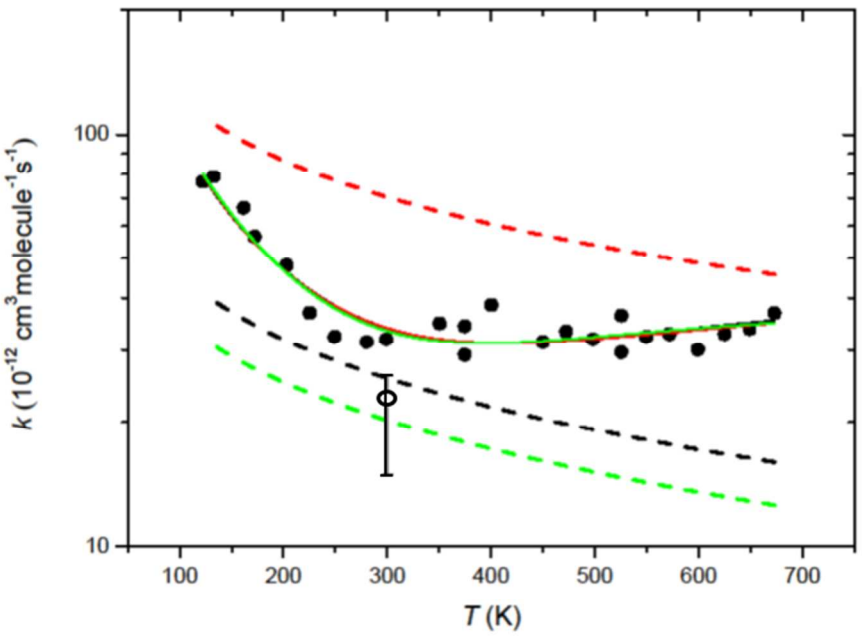

Fig.7

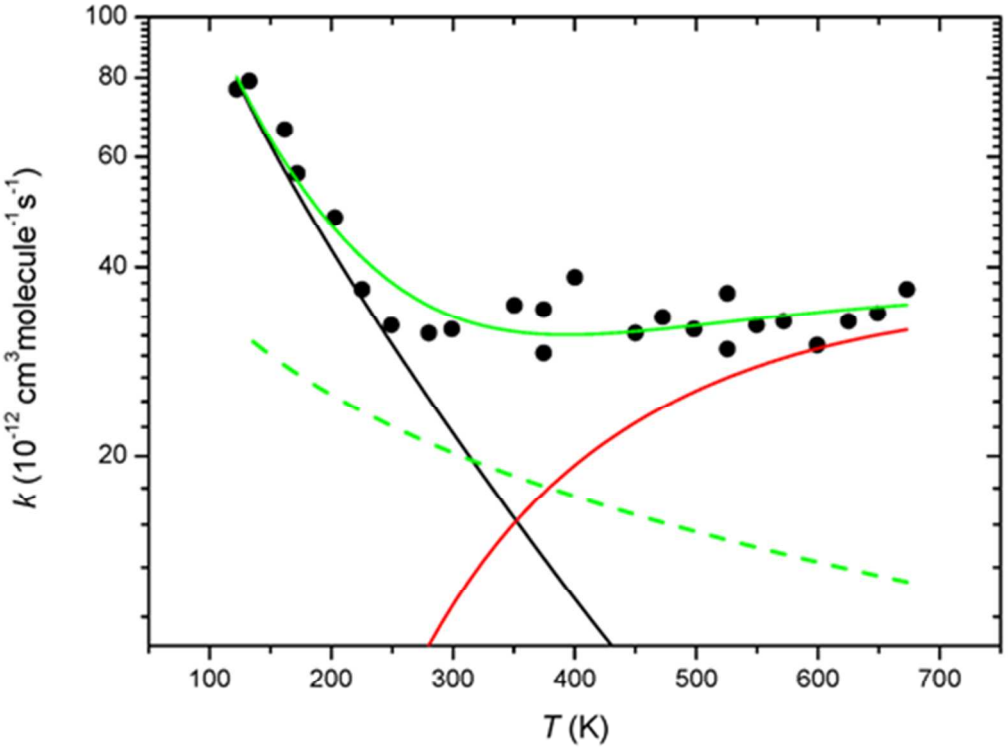

Fig. 8

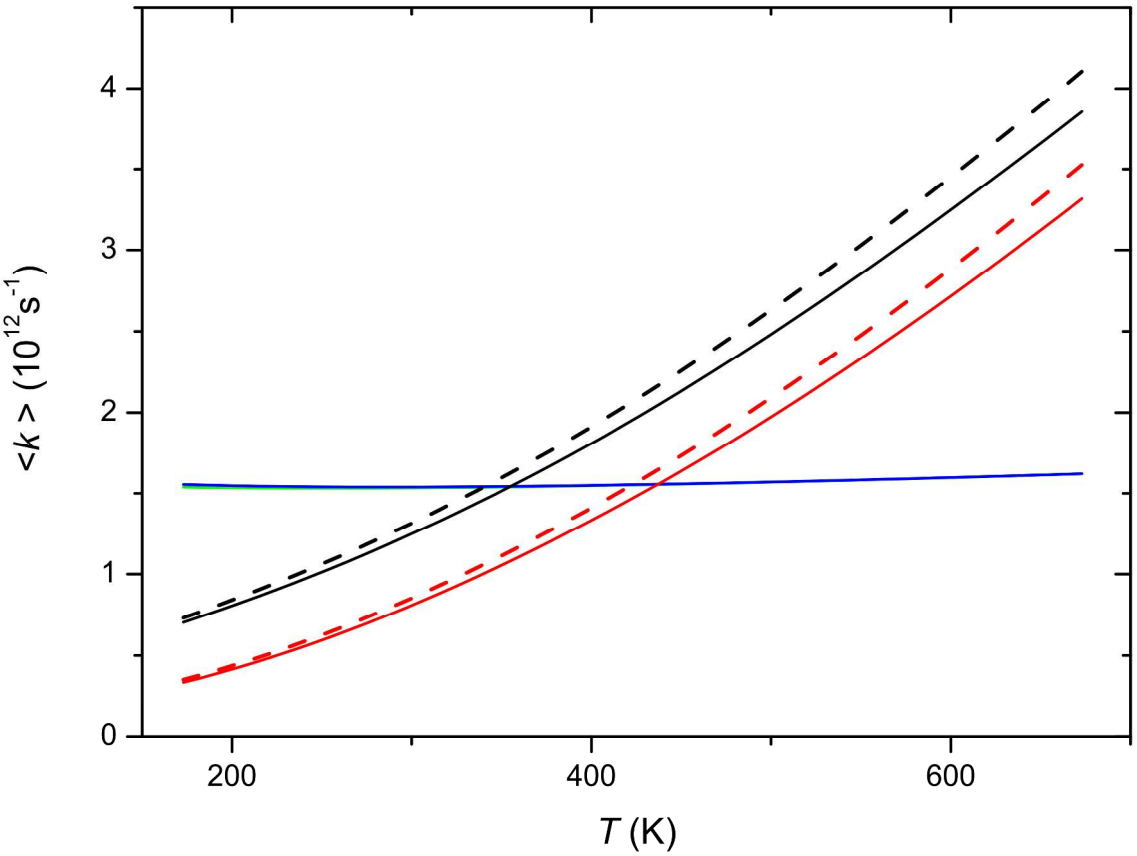

Fig. 9